CrystEngComm

PAPER

View Article Online
View Journal | View Issue

Cite this: *CrystEngComm*, 2016, **18**, 3585

Shape-controlled hydrothermal synthesis of superhydrophobic and superoleophilic $BaMnF_4$ micro/nanostructures†

Yong Chen,[a] Feng Li,*[a] Taohai Li[a] and Wei Cao[b]

Received 21st December 2015,
Accepted 11th April 2016

DOI: 10.1039/c5ce02502h

www.rsc.org/crystengcomm

In this paper, we focus on the controllable synthesis of $BaMnF_4$ micro/nanostructures *via* a facile one-step hydrothermal method assisted by different surfactants. The chemical structure, morphology and superhydrophobic properties have been studied by XRD, SEM, TEM, EDS and CA. The results show that the pH of the starting solution, temperature, reaction time, and surfactant affect the crystallinity, morphology and superhydrophobic properties of the products. The preliminary reaction path and formation mechanisms of the $BaMnF_4$ with different shapes are also investigated. To the best of our knowledge, the present synthesis route is novel. Furthermore, the as-prepared $BaMnF_4$ surface shows superhydrophobicity and superoleophilicity.

Introduction

Barium manganese fluoride, $BaMnF_4$, is a classical ferroelectromagnet which has unusual magnetic and electrical properties and has been the subject of intensive research in the past decades.[1–6] It belongs to the isostructural family of barium fluorides with the chemical formula of $BaMF_4$, where M can be Mn, Fe, Co, Ni, Zn, or Mg.[7] These multiferroic materials which have simultaneous ferroelectric, ferromagnetic or ferroelastic ordering have aroused a lot of interest due to their potential for applications in advanced devices, such as memory devices, read–write devices, data storage *etc.*[8–10] Due to their unique magnetic and dielectric properties, multiferroics have vast potential for technological applications.[11–13] In addition, due to their high transparency, these fluorides can be used as optical materials.[14–16]

So far, numerous approaches to synthesize $BaMF_4$ materials have been reported, such as the high solid-state method, sol–gel methods, high-temperature hydrothermal methods, and so on.[17–21] Originally, Eibschütz, M. *et al.* fabricated the $BaMF_4$ family of materials which were grown as crystals from the melt of BaF_2 and MF_2 in HF atmosphere above 800 °C.[17] Then, Recker, K. *et al.* synthesized single crystals of $BaMgF_4$ by Czochralski and Bridgeman's methods.[18] In these reports, either CF_4 or anhydrous HF gas was used at about 920 °C. After that, Fujihara, S. *et al.* employed the sol–gel method to synthesize polycrystalline $BaMgF_4$; but in this report, BaF_2 and/or MgF_2 impurities were found.[20] In short, these methods require not only complicated equipment, but also strict conditions, such as high temperature, high cost, long time, and so on. Meanwhile, the as-synthesised products are not pure. Sun Woo Kim *et al.* first succeeded in the preparation of pure and polycrystalline $BaMF_4$ (M = Mg, Mn, Co, Ni or Zn) by a convenient low-temperature (about 230 °C) hydrothermal route.[22] And the method avoids the use of HF by using a milder fluorinating agent, CF_3COOH, in an aqueous medium. But CF_3COOH is also dangerous and toxic, and the temperature is also high. Sayed, F. N. *et al.* reported a new fluoride-based series of materials with the general composition of $BaMg_{1-x}Mn_xF_4$ ($0.0 \leq x \leq 0.15$), synthesized by a hydrothermal method.[23] Farheen N. Sayed developed an environmentally friendly and mild hydrothermal synthesis of fluoride-based materials ($BaMF_4$ (M = Co, Ni, Zn)).[24] Despite the rather simple methods, the products are not pure either. And these papers mostly focused on their physical properties like magnetic, electrical and optical properties, while their morphology and superhydrophobicity were not reported.

In this paper, we focus on the controllable synthesis of $BaMnF_4$ micro/nano-structures *via* a facile one-step hydrothermal method assisted by different surfactants. The $BaMnF_4$ bundles and microspheres we obtained have perfect monodispersity, uniformity, and well-defined crystallographic facets. To the best of our knowledge, this way of synthesizing $BaMnF_4$ bundles and microspheres at such a low temperature has never been reported in the literature. The chemical

[a] *College of Chemistry, Key Laboratory of Environment-Friendly Chemistry and Applications Ministry of Education, Xiangtan University, Xiangtan, China. E-mail: fengli_xtu@hotmail.com; Fax: +86 731 58292251; Tel: +86 731 58292202*
[b] *Nano and Molecular Systems Research Unit, University of Oulu, P.O. Box 3000, FIN-90014, Finland*

† Electronic supplementary information (ESI) available: EDX spectrum of $BaMnF_4$; CAs of water droplets on the glass not modified and modified by stearic acid; superoleophilicity and superhydrophobicity movies. See DOI: 10.1039/c5ce02502h

structure, morphology and superhydrophobicity have been studied by XRD, SEM, TEM, EDS and CA. The results show that the pH of the starting solution, temperature, reaction time and surfactant affect the crystallinity, morphology and superhydrophobic properties of the products. The preliminary reaction path and formation mechanisms of $BaMnF_4$ with different shapes were also investigated. Moreover, we report the wettability of the $BaMnF_4$ samples and found that the as-prepared $BaMnF_4$ samples absorb oil quickly, but repel water completely.

Experimental

Materials and synthesis

All reagents were of analytical grade, purchased from Shanghai Chemical Reagent Factory, and used as received without further purification. In a typical synthesis, $BaCl_2{\cdot}2H_2O$ (2 mmol) and $MnCl_2{\cdot}2H_2O$ (2 mmol) were dissolved in 15 mL of distilled water, followed by adding NH_4F (8 mmol) under magnetic stirring. After stirring for 30 min at room temperature, this homogeneous mixture was then transferred into a Teflon-lined stainless-steel autoclave of 20 mL capacity and heated at different temperatures for different durations. After cooling down, the $BaMnF_4$ products were collected by centrifugation, washed with anhydrous ethanol and distilled water, and finally dried in air at 70 °C for 12 h. The surfactant, pH, reaction time, and temperature were found to be very crucial for the formation and crystallization of the monophasic products.

A glass slide substrate was vertically placed in the reaction solution after being ultrasonically cleaned in acetone, absolute ethanol and distilled water for 10 min each, using an ultrasonic cleaner at a frequency of 50 kHz. The superhydrophobic surface was prepared *via* a facile drop-casting method: first, a glass surface was modified by slow evaporation of a dilute $BaMnF_4$ ethanol dispersion, followed by drying at room temperature. In the second step, the films on the glass substrates were modified by adding a 5 mM stearic acid hexane solution, followed by drying at 120 °C for 1 h.

Characterization

The obtained samples were characterized by X-ray powder diffraction (XRD) using a MiniFlex II X-ray diffractometer operated at 40 kV and 40 mA using Cu K radiation (λ = 0.15406 nm). The scanning electron microscopy (SEM) images were obtained on a JEOL JSM-6360. Thermogravimetric analysis (TGA) curves were studied on a TGA 50 thermogravimetric analyzer at a heating rate of 20 °C min^{-1} in dynamic nitrogen atmosphere (60 ml min^{-1}). Water contact angle (CA) and sliding angle measurements were carried out at ambient temperature by an optical contact angle meter (250-F1). Water droplets (5 μL) were carefully dropped onto the surfaces, and an average value of five measurements obtained at different positions in the samples was used as the final contact angle.

Results and discussion

$BaMnF_4$ was synthesized from the reaction of $BaCl_2$, $MnCl_2$ and NH_4F in a water bath. In order to investigate the effects of the pH values of the starting solution, temperature, reaction time and surfactants on the crystallinity, morphology and superhydropholicity of the samples, a series of controlled experiments were carried out. In the synthesis of these compounds, NH_4F has several functions. For example, it is a fluorinating agent and assists to keep the pH of the solution while the F^- ions are efficient mineralizers.[25]

Moreover, NH_4F, which is safe to handle, was used instead of highly corrosive HF which is chemically hazardous due to its corrosive nature.

Effects of the pH value on phase purity

Fig. 1 shows the XRD patterns of the samples prepared *via* the hydrothermal method under different pH conditions at 160 °C for 24 h. As presented in Fig. 1a, almost all the diffraction peaks could be perfectly indexed to the $BaHF_3$ (JCPDS 35-1378) at the pH value of 1, which shows that the prepared $BaHF_3$ samples are single-phase.[26] When the pH increases to 4, all visible peaks can be assigned to the standard crystal structure, indicating the formation of $BaMnF_4$ at the pH value of 4 (JCPDS 21-0077) (Fig. 1b).[27] That is to say, $BaMnF_4$ has been obtained at the pH value of 4.

As the pH increases to 7, the phase of the samples coincides with that of the BaF_2 (JCPDS 85-1341) (Fig. 1c).[28] Then, the pH is increased to 13 and the XRD patterns also coincide with that of the BaF_2. The above statements indicate that only when the pH value reaches 4 can the $BaMnF_4$ be acquired. It suggests that the pH plays a crucial role during the synthesis of $BaMnF_4$. The EDX spectrum is further used to determine the chemical composition of the as-synthesized products at the pH value of 4 (see the ESI,† Fig. S1). The results show that the product chiefly consists of Ba, Mn, and F.

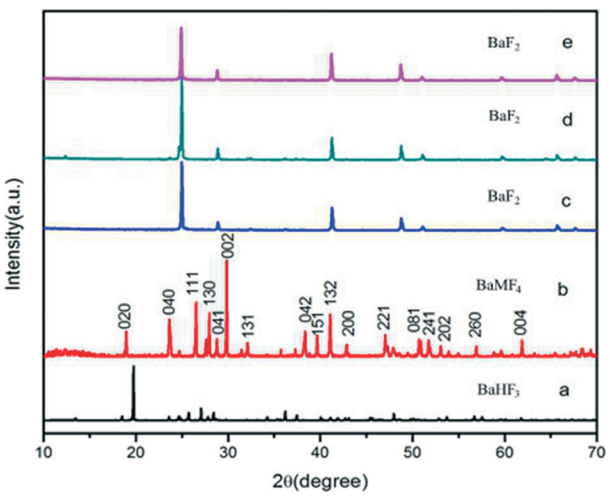

Fig. 1 XRD patterns of the samples prepared *via* the hydrothermal method under different pH conditions at 160 °C for 24 h. (a) pH = 1, (b) pH = 4, (c) pH = 7, (d) pH = 10, (e) pH = 13.

This further demonstrates that the as-synthesized products at the pH value of 4 are pure.

Effects of reaction temperature on phase impurity and morphology

XRD analysis is employed to detect the phase evolution of the products during the variation of hydrothermal temperatures. Fig. 2 shows the XRD patterns of the samples prepared *via* hydrothermal methods at different temperatures for 24 h. As presented in Fig. 2a, all diffraction peaks are in good agreement with the $BaMnF_4$ structure (JCPDS 21-0077) and no other diffraction peaks are detected. The diffraction peaks are narrow and sharp, indicating that the product is of high crystallinity. The results indicate that the $BaMnF_4$ samples can be synthesized by this facile method at 160 °C. When the temperature was increased to 180 °C, all peaks except the peak at 25° correspond to the $BaMnF_4$ crystal structure. These additional peaks are attributed to BaClF (JCPDS 34-0674), indicating the presence of a $BaMnF_4$/BaClF hybrid structure in the synthesized products.[29] When the temperature declined to 140 °C, all peaks except the peak at 25° correspond to the $BaMnF_4$ crystal structure, too. The above statements indicate that the suitable growth temperature has a narrow range. Higher or lower ones are detrimental to the synthesis of $BaMnF_4$. This XRD results indicate that reaction temperature plays a crucial role in controlling the phase composition of the final products.

Fig. 3 shows the SEM images of the as-synthesized products after hydrothermal treatment at 140 °C, 160 °C, and 180 °C for 24 h. As the hydrothermal temperature was increased to 160 °C, $BaMnF_4$ bundles with a length of about 43 μm and width of about 10 μm were formed by oriented nanorods (Fig. 3b). The as-obtained bundles cannot be destroyed or broken into discrete individual nanorods even by subjecting their aqueous suspension to long-term ultrasonication, which indicates that the microspheres are not a random aggregate

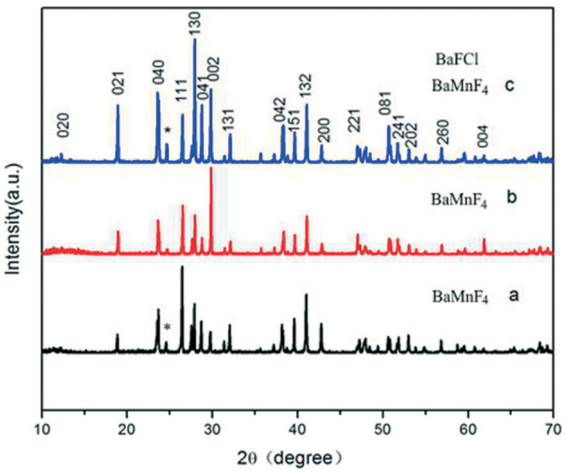

Fig. 2 XRD patterns of the samples prepared *via* the hydrothermal method at different temperatures for 24 h. (a) 140 °C, (b) 160 °C, (c) 180 °C.

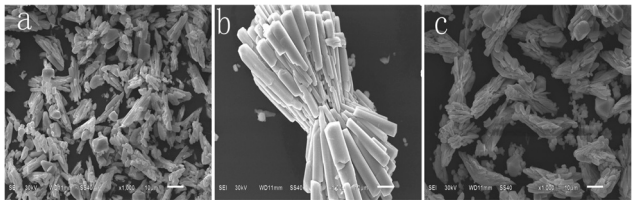

Fig. 3 The SEM images of the as-synthesized products after the hydrothermal treatment at different temperatures for 24 h. (a) 140 °C, (b) 160 °C, (c) 180 °C.

of nanorods, but are an ordered self-assembly.[30] Further increase in the hydrothermal temperature to 180 °C causes the bundle structure volume to decrease (Fig. 3c). Meanwhile, there is a small amount of polyhedral particles at this temperature. Fig. 3a reveals that further decrease in the hydrothermal temperature to 140 °C leads to the formation of an inhomogeneous product with a predominantly aggregated bulk. However, many dispersed particles appeared. This result is possibly due to the fact that the hydrothermal temperature of the composite materials provided the driving force that primarily affects the progress of the reaction and crystallization rate, which affects the quality and morphology of the crystals.[31]

For further analysis, the as-synthesized $BaMnF_4$ bundles are characterized by the TEM and the results are presented in Fig. 4. Fig. 4(a) and (b) show the TEM images of the $BaMnF_4$ bundles which confirm that the bundles with a length of about 43 μm and width of about 10 μm are formed by oriented nanorods, which is in good agreement with the former SEM images. A high-resolution TEM (HRTEM) image of $BaMnF_4$ bundles is shown in Fig. 4(c) and the clear lattice fringe indicates the good crystalline and single crystalline characteristics of the bundles. The lattice interplanar spacings are 0.377 and 0.337 nm, corresponding to the (040) and (111) planes, which is in good agreement with the former XRD pattern.[27]

Effects of reaction time

Fig. 5 shows the XRD patterns of the samples prepared *via* the hydrothermal method at 160 °C for different reaction times. As presented in Fig. 5a, all diffraction peaks are in good agreement with the $BaMnF_4$ structure (JCPDS No. 21-0077) and no other diffraction peaks are detected. The

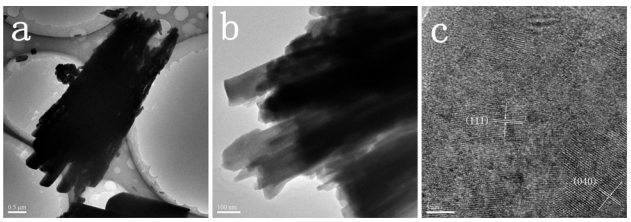

Fig. 4 (a), (b) TEM images of the $BaMnF_4$ bundles; (c) typical HRTEM image of the edge of the $BaMnF_4$ bundles.

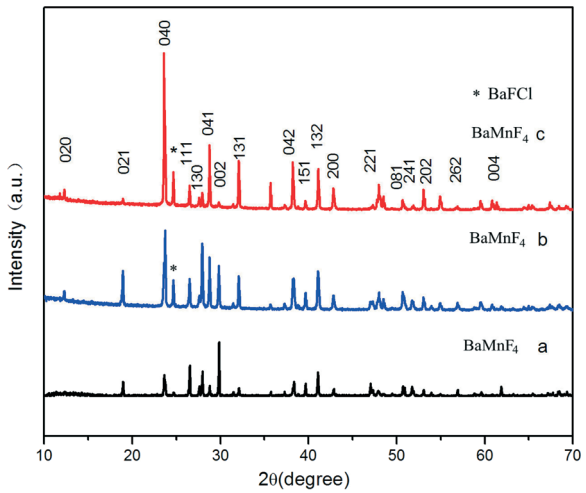

Fig. 5 The XRD patterns of the samples prepared *via* the hydrothermal method at 160 °C for different reaction times. (a) 24 h, (b) 48 h, (c) 72 h.

diffraction peaks are narrow and sharp, indicating that the product is of high crystallinity. When the reaction time increases up to 48 h, all peaks except the peaks at 25° correspond to the $BaMnF_4$ crystal structure. These additional peaks are attributed to BaClF (JCPDS file no. 34-0674), indicating the presence of a $BaMnF_4$/BaClF hybrid structure in the synthesized products. Prolonging the reaction time to 72 h, all peaks except the peaks at 25° correspond to the $BaMnF_4$ crystal structure, too. Simultaneously, the intensity of this peak increases for the composites with increasing reaction time. It indicates that the BaFCl crystal growth rate will be faster than the $BaMnF_4$ with the extension of reaction time. From the above results, it can be clearly seen that the reaction time has significant effects on controlling the phase composition of the final products.

Fig. 6 shows the SEM images of the samples prepared *via* the hydrothermal method at 160 °C for different reaction times. As presented in Fig. 5a, the $BaMnF_4$ bundles prepared for 24 h is composed of nanorods with a length of about 43 μm and width of about 10 μm. Further increase in the reaction time to 48 h causes the nanorod volume to decrease (Fig. 6b) and a few fragmentary nanorods appear. However, further increase in the reaction time to 72 h causes most of the bundles to fracture. Furthermore, there are many fragmentary nanorods and particles. This result is possibly due to the fact that most bundles dissolve, form new growth units, renucleate, and then crystallize, which leads to the formation of other morphologies and phases.[32] From the above results, it can be clearly seen that the reaction time affects the phase and morphology of the final products.

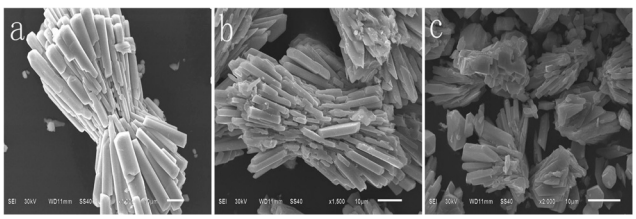

Fig. 6 The SEM images of the samples prepared *via* the hydrothermal method at 160 °C for different reaction times. (a) 24 h, (b) 48 h, (c) 72 h.

Effects of surfactant

The morphologies of the as-prepared products at 160 °C for 24 h with different reaction surfactants are investigated by examining the SEM images (Fig. 7). The obvious changes in the morphology are observed in Fig. 7a–f. The images show that the addition of surfactants plays a critical role in the morphology of the samples. Without the addition of a surfactant, $BaMnF_4$ bundles with a length of about 43 μm and width of about 10 μm are formed by oriented nanorods. And their surface is smooth (Fig. 7a). However, once hexadecyl trimethyl ammonium bromide (CTAB) is introduced into the reaction system, the morphology changes tremendously. Many irregular lamellar structures appear, and there are a large number of irregular small particles and small lumps (Fig. 7b). As shown in Fig. 7c, the prepared samples with ethylene diamine tetraacetic acid (EDTA) as the surfactant gradually change to microspheres which are composed of many aligned single-crystalline nanorods with a length of about 20 μm and width of about 0.6 μm. This may be because EDTA suppresses the nucleation process of the product, also promotes the crystallization process, eventually leading to the formation of the obtained product with developed crystals.[33] The spindle structure sample consisting of uniform flakes is

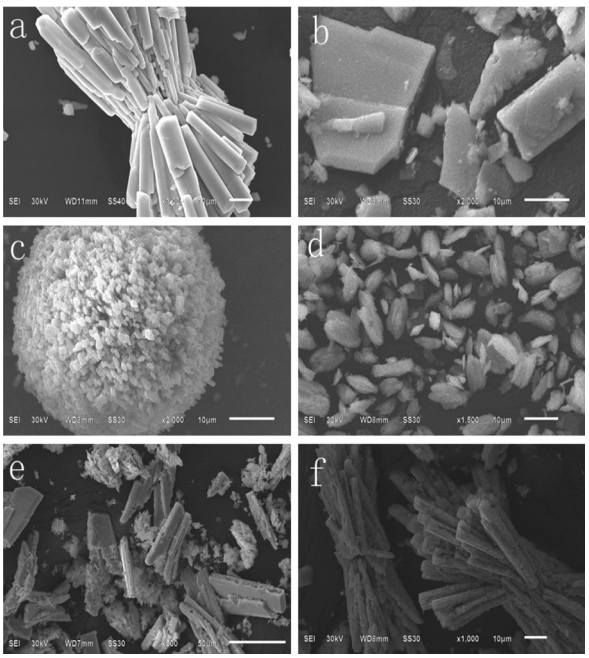

Fig. 7 The SEM images of the samples prepared at 160 °C for 24 h with different reaction surfactants: (a) no surfactants, (b) CTAB, (c) EDTA, (d) citric acid, (e) L-glutamate, (f) PVP.

achieved when citric acid is used as the template (Fig. 7d), and the average length of the sample is about 7 μm and the width is about 3 μm. This means that citric acid may promote the nucleation and crystallization process of $BaMnF_4$ to form the uniform flake structures.[34] Fig. 7e shows the typical SEM images for products prepared with L-glutamate as the surfactant. The morphology of the products is similar to the original morphology and only their surface is significantly rougher than that of the original. As shown in Fig. 7f, the prepared sample with polyvinylpyrrolidone (PVP) as the surfactant is almost composed of bundle structure crystals, but many irregular agglomerated particles appeared. PVP may play an important role in the growth units of the sample, which can promote the nucleation in the preliminary reaction and restrain the crystallization process of the particles.[35] In this work, we speculate that in the growing process of $BaMnF_4$ microcrystals, the surfactant binds to the surfaces selectively as a shape modifier. Hence, we can say that the surfactant can be adsorbed on the crystal surfaces of the $BaMnF_4$ products effectively, and it can control the growth of the $BaMnF_4$ microcrystals as the capping agent. Through using different surfactants, $BaMnF_4$ microcrystals with different shapes and sizes can be obtained.

Reaction path

Based on the above results, we are apt to describe the crystal reaction path of the $BaMnF_4$ prepared as one involving a sequence of dissolution, nucleation, redissolution and recrystallization. The possible formation process under hydrothermal conditions can be expressed as follows:

$$BaCl_2 + NH_4F \rightarrow BaFCl + NH_4Cl \quad (1)$$

$$BaFCl + NH_4 \rightarrow BaF_2 + NH_4Cl \quad (2)$$

$$Mn^{2+} + 4F^- \rightarrow MnF_4{}^{2-} \quad (3)$$

$$MnF_4{}^{2-} + Ba^{2+} \rightarrow BaMnF_4 \quad (4)$$

$$BaF_2 + HF \rightarrow BaHF_3 \quad (5)$$

In the process of the preparation of a precursor solution, first, Ba^{2+} combines with Cl^- and F^- in an aqueous solution forming BaFCl (reaction (1)). With the addition of NH_4F, BaFCl continues to react with it, and removes Cl^- forming BaF_2 (reaction (2)). When NH_4F exists in solution, Mn^{2+} first combines with F^- to form $MnF_4{}^{2-}$ species. Then it reacts with Ba^{2+} forming the desired product $BaMnF_4$ (reaction (3) and (4)). The NH_4F solution is weakly acidic because of its hydrolysis, which is in good agreement with earlier experimental results (only when the pH value equals 4 can $BaMnF_4$ be synthesised). When HF is added to the solution, the solution becomes too acidic. The excess acidity causes the generation of $BaHF_3$ (reaction (5)), which is consistent with the XRD results ahead. When $NH_3{\cdot}H_2O$ is added to the solution, the solution becomes neutral or alkaline, which hinders reactions (3) and (4) to form BaF_2 under neutral and alkaline conditions, which is consistent with earlier experimental results (when pH = 7, 10 and 13, BaF_2 is synthesised). BaFCl impurities appeared more than once in the previous experiment, which is related to reaction 1.

These mechanisms are verified through a large number of exploratory experiments and XRD tests.

Formation mechanism for different morphologies of products

In order to understand the formation process of $BaMnF_4$ bundles, time-dependent experiments were carefully conducted. Fig. 8 shows the SEM images of the samples without surfactants hydrothermally synthesized at 160 °C for 1, 2, 4, 8, 24 and 48 h. As can be seen from Fig. 8a, the products are irregular amorphous aggregates within the initial 1 h. And these aggregates can be made up of some small nanonucleations. As the reaction time extends to 2 h, these aggregates are transformed into irregular microrods. Meanwhile, many irregular particles appear, maybe because there is not enough time to form nanorods. After 4 h of growth, the microrods self assemble into straw-like bundles, and most of their ends are pointed. As the reaction time increases to 8 h, the straw-like bundles tend to form completely and most of the cutting-edges disappear, but still produce a lot of shapeless particles. With the reaction time increasing to 24 h, the straw-like bundles become more regular, and the shapeless particles disappear. Based on the above analysis, the formation of the present structures is assigned to the Ostwald ripening mechanism. The formation mechanism of the $BaMnF_4$

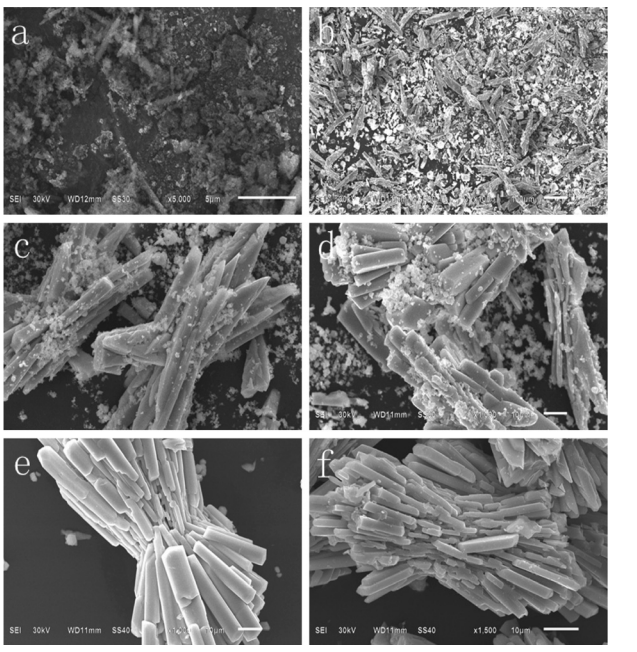

Fig. 8 SEM images of the samples without surfactants hydrothermally synthesized at 160 °C for (a) 1 h, (b) 2 h, (c) 4 h, (d) 8 h, (e) 24 h, (f) 48 h.

bundles is deduced as follows. First, amorphous aggregates slowly form crystal nuclei. Due to the intrinsic anisotropic growth habit of $BaMnF_4$, these first-born crystal nuclei develop into nanorods under hydrothermal conditions. Then, the microrods self assemble into straw-like bundles. As the reaction proceeds, straw-like bundles grow up gradually, and micro/nanoparticles disappear. Finally, the product with bundle-like structures is obtained, and their surfaces are smooth. According to the above description, the whole formation of $BaMnF_4$ nanorod-bundles can be summarized in the schematic illustration as shown in Fig. 9.

Fig. 10 shows the SEM images of the samples with EDTA as a surfactant hydrothermally synthesized at 160 °C for 1, 2, 4, 8, 24, and 48 h. First, Ba^{2+} and Mn^{2+} react with EDTA in aqueous solution to form the stable complex Ba–EDTA–Mn. As the hydrothermal reaction proceeds, Ba–EDTA–Mn decomposes and combines with F^-, generating the product $BaMnF_4$. When the hydrothermal reaction begins, Ba–EDTA–Mn decomposes and combines with the F^- ions to form a number of nanocrystals of $BaMnF_4$. Because nanocrystals have a tendency to reunite, some nanocrystals begin to reunite into granules under the driving force of the minimization of the total energy of the system (Fig. 10a). As the reaction time extends to 2 h, many irregular dumbbell-like structures appear. After 4 h of growth, the microrods self assemble into spiny spheres. As the reaction time increased to 8 h, the spiny spheres tend to form completely and transform into microspheres. With the reaction time increasing to 24 h, the microspheres tend to form completely. Further increase in the reaction time to 48 h results in their surfaces becoming smooth. Based on the above analysis, the formation of the present structures is assigned to the Ostwald ripening mechanism as well. The formation mechanism of $BaMnF_4$ microspheres is deduced as follows. First, amorphous aggregates form dumbbells of self-assembled nanorods. As the reaction proceeds, the dumbbells develop into spiny spheres, and the unformed micro/nano particles disappear. Finally, microspheres are obtained, and their surfaces are smooth. According to the above description, the whole formation of $BaMnF_4$ nanorod-bundles can be summarized in the schematic illustration as shown in Fig. 11.

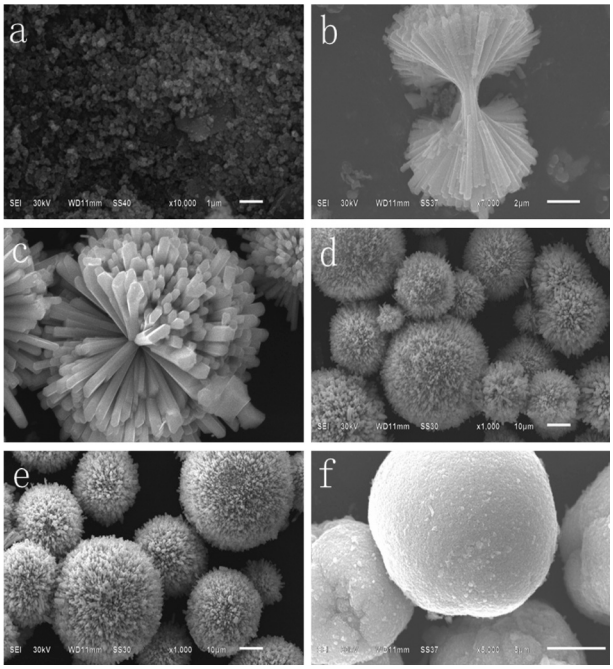

Fig. 10 SEM images of the samples with EDTA as a surfactant hydrothermally synthesized at 160 °C for (a) 1 h, (b) 2 h, (c) 4 h, (d) 8 h, (e) 24 h, (f) 48 h.

Wettability of the $BaMnF_4$ film

Fig. 12 shows the CAs of water droplets on the surfaces of different $BaMnF_4$ samples synthesized at different temperatures for 24 h. As shown in Fig. 12a–c, the CA values of 166.32°, 152.66° and 167.50° correspond to the temperatures of 140 °C, 160 °C, and 180 °C, respectively. Also, we measured the CAs of the water droplets on the surfaces of glass and glass modified by stearic acid, and the CA values are 63.22° and 74.65°, respectively (Fig. S2†). Therefore, the wettability of the glass modified by $BaMnF_4$ samples and stearic acid improved greatly and it achieved superhydrophobicity. These CA results confirm that the surface wettability of $BaMnF_4$ can be tuned *via* changing the reaction temperature. The CA values of (a) and (c) surfaces are larger than that in (b); this is mainly because at 160 °C, the product purity and crystallinity are high, and the content of impurities is rare, leading to samples of a large volume and smooth surface. While at 140 °C and 180 °C, there are more product impurities, and the sample volume was obviously reduced, making the degree of roughness of the surface increase, conducive for improving their hydrophobicity. And all of these are in good agreement with the former SEM and XRD pattern.

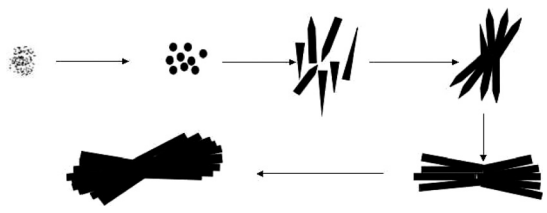

Fig. 9 Schematic illustration of the growth process of $BaMnF_4$ bundles.

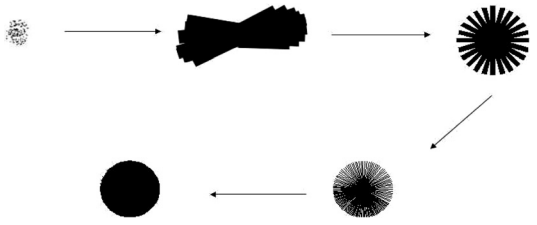

Fig. 11 Schematic illustration of the growth process of $BaMnF_4$ microspheres.

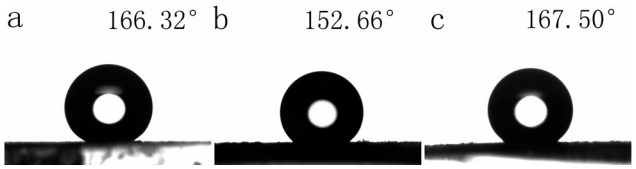

Fig. 12 Water droplets on the surfaces of different $BaMnF_4$ samples synthesized at different temperatures for 24 h. (a) 140 °C, (b) 160 °C, (c) 180 °C.

Fig. 13 shows the CAs of the water droplets on the surfaces of different $BaMnF_4$ samples synthesized at 160 °C for different reaction times. As shown in Fig. 13a–c, the CA values of 152.66°, 152.44° and 153.68° correspond to the temperature of 24 h, 48 h, and 72 h, respectively. The CA values of (a), (b), and (c) surfaces are similar to each other and are larger than 150°, which is in good agreement with their morphologies having similar SEM images.

Additionally, the oil wettability of the original and the as-prepared $BaMnF_4$ sample synthesized at 160 °C for 24 h is also examined through the contact angle measurement. Fig. 14 shows a drop of octane absorbed by the as-prepared $BaMnF_4$ sample. In movie S1,† we get a drop of octane on the as-prepared $BaMnF_4$ sample. The octane spreads quickly on the coating and is absorbed thoroughly within about 1.5 s, which shows that the as-prepared $BaMnF_4$ samples absorb oil quickly, but repel water completely.

We carry out a rolling test of water droplets. In movie S2,† we get a drop of water (dyed with RhB) on the as-prepared $BaMnF_4$ sample. Video snapshots of a drop of water rolled on the as-prepared $BaMnF_4$ sample at 160 °C for 24 h are shown in Fig. 15. Fig. 15 shows that the water sliding angle on the surface is less than 5° and that the droplet can rapidly escape from left to right. This result is possibly because the micro/nanostructure of the as-prepared films and the low surface energy of stearic acid led to the reduction of the adhesion force to the water droplets.[36]

Though there are a lot of methods for preparing superhydrophobic surfaces, most of them are suffering from the binding force problem. That is to say, the modified surface is easily peeled off the basement after concussion, leading to the loss of superhydrophobicity. To thoroughly investigate the binding force with the substrate, the modified surface was ultrasonically cleaned with distilled water for 3 h, and then dried in air at 70 °C for 12 h. After ultrasonic concussion, the morphology of the as-prepared surface became similar to the original morphology and there is no significant change in superhydrophobicity (Fig. S3†).

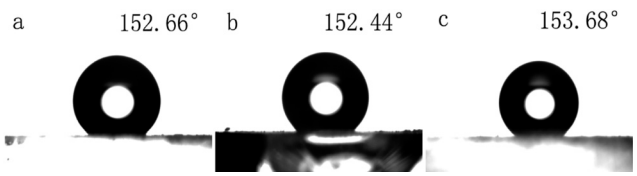

Fig. 13 CAs of the water droplets on the surfaces of different $BaMnF_4$ samples synthesized at 160 °C for different reaction times. (a) 24 h, (b) 48 h, (c) 72 h.

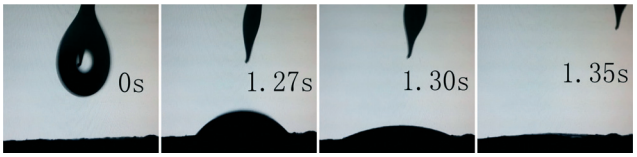

Fig. 14 Video snapshots of a drop of octane absorbed by the as-prepared $BaMnF_4$ sample synthesized at 160 °C for 24 h.

We next conducted a scratch test to thoroughly investigate the mechanical durability of the superhydrophobic surfaces. The process of the abrasion test is illustrated in Fig. 16a. The superhydrophobic surface, enduring a pressure of 2000 Pa, was dragged across the surface of a SiC sandpaper (1200 mesh) in one direction with a speed of 1 cm s^{-1}. Fig. 16b displays that the as-prepared surface still maintained the CA above 150° after 1000 mm of abrasion. Despite that, the as-prepared surface showed good mechanical durability. Additionally, after being pressed with a finger, the $BaMnF_4$ surface remained superhydrophobic (see Fig. S4†). The water droplets maintained a spherical shape on the surface and could easily roll off at a small sliding angle. To some extent, these results revealed that the as-prepared surface exhibited good mechanical stability.

Superhydrophobic surfaces have great potential applications in liquid transportation without any loss, especially for some expensive liquids.[37] Thus the design of a pH resistant superhydrophobic surface under different pH conditions is important to expand the applications. And we also use different substrates to explore the relationship between the base and water CA on the surface.

Table 1 shows the relationship between the pH value of the water droplet and CA on the superhydrophobic surfaces. When the pH value was from 1 to 13, the CA values are all

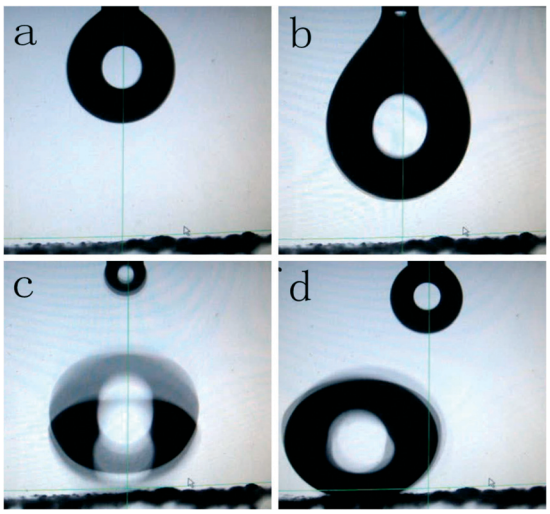

Fig. 15 Video snapshots of a sliding water droplet on the surface in chronological order (a–d) formed by the $BaMnF_4$ sample synthesized at 160 °C for 24 h.

Fig. 16 (a) Schematic diagram of the abrasion test; (b) photo of abrasion test and (c) water droplets exhibiting a spherical shape on the scratch surface.

Table 1 Water contact angles of the modified resulting surface according to the pH of the water droplet

pH	CA (°)
1	153.26
3	160.15
5	160.32
7	167.50
9	159.82
11	158.26
13	150.56

larger than 150°. These results indicate that the superhydrophobicity of the as-prepared films are very stable under either acidic or basic conditions.

Furthermore, the environmental durability and stability of the superhydrophobic property of the films were checked after exposure to the atmosphere for 3 months. The water CA on the surface remains larger than 150° after storage for three months at ambient temperature, and the SA is less than 5°. This indicates the long-term stability of the film.

Conclusions

In this work, $BaMnF_4$ micro/nano-structures of different morphologies are synthesized *via* a facile one-step hydrothermal method assisted by different surfactants. Through adjusting the synthetic parameters (such as pH of the starting solution, temperature, reaction time, and surfactant), monodisperse $BaMnF_4$ bundles and microspheres have been synthesized successfully. The preliminary reaction path and formation mechanisms of $BaMnF_4$ for the different shapes are also investigated *via* time-dependent experiments and some other experiments. Moreover, we have reported the wettability of the $BaMnF_4$ samples and found that the as-prepared BaMnF4 samples absorbed oil quickly, but repelled water completely. The results show that the materials presented long-term stability in air as well as excellent resistance to corrosive liquids, including weakly acidic, alkaline reagents. These superhydrophobic and superoleophilic films may be applied to some fields (such as oil mixture separation, self-cleaning materials, drag-reducing materials, and so on) and have promising commercial applications.

Acknowledgements

The authors acknowledge with thanks the financial support from the Provincial Natural Science Foundation of Hunan, China (2015JJ2138), the Open Project Program of the State Key Laboratory of Structural Chemistry, China (No. 20150018), the National Natural Science Foundation of China (21343008) and the Oulu University Strategic Grant. T. Li acknowledges the Oulu University Short-term International Research Visit grant during his stay in Finland.

Notes and references

1 H. G. von Schnering and P. Bleckmann, *Naturwissenschaften*, 1968, **55**, 342–343.
2 E. T. Keve, S. C. Abrahams and J. L. Bernstein, *J. Chem. Phys.*, 1969, **51**, 4928–4936.
3 D. E. Cox, M. Eibschütz, H. J. Guggenheim and L. Holmes, *J. Appl. Phys.*, 1970, **41**, 943–945.
4 E. T. Keve, S. C. Abrahams and J. L. Bernstein, *J. Chem. Phys.*, 1970, **53**, 3279–3287.
5 A. H. Arkenbout, T. T. M. Palstra, T. Siegrist and T. Kimura, *Phys. Rev. B: Condens. Matter Mater. Phys.*, 2006, **74**, 184431.
6 J. F. Scott, *Rep. Prog. Phys.*, 1979, **42**, 1055.
7 X. Wang, S. Fujihara, T. Kimura and H. Chen, *Ferroelectrics*, 2001, **264**, 121–126.
8 N. A. Spaldin and M. Fiebig, *Science*, 2005, **309**, 391–392.
9 D. Khomskii, *Physics*, 2009, **2**, 20.
10 M. Bibes and A. Barthélémy, *Nat. Mater.*, 2008, **7**, 425–426.
11 W. Prellier, M. P. Singh and P. Murugavel, *J. Phys.: Condens. Matter*, 2005, **17**, R803.
12 N. A. Hill, *J. Phys. Chem. B*, 2000, **104**, 6694–6709.
13 M. Osada and T. Sasaki, *Adv. Mater.*, 2012, **24**, 210–228.
14 J. M. Rey, H. Bill, D. Lovy and H. Hagemann, *J. Alloys Compd.*, 1998, **268**, 60–65.
15 K. Shimamura and E. G. Víllora, *J. Fluorine Chem.*, 2011, **132**, 1040–1046.
16 E. G. Víllora, K. Shimamura, K. Sumiya and H. Ishibashi, *Opt. Express*, 2009, **17**, 12362–12378.
17 M. Eibschütz and H. J. Guggenheim, *Solid State Commun.*, 1968, **6**, 737–739.
18 K. Recker, F. Wallrafen and S. Haussühl, *J. Cryst. Growth*, 1974, **26**, 97–100.
19 E. Banks and A. M. Srivastava, *J. Electrochem. Soc.*, 1987, **134**, 1568–1570.
20 S. Fujihara, S. Ono, Y. Kishiki, M. Tada and T. Kimura, *J. Fluorine Chem.*, 2000, **105**, 65–70.
21 C. Ederer and N. A. Spaldin, *Phys. Rev. B: Condens. Matter Mater. Phys.*, 2006, **74**, 024102.
22 S. W. Kim, H. Y. Chang and P. S. Halasyamani, *J. Am. Chem. Soc.*, 2010, **132**, 17684–17685.
23 F. N. Sayed, B. P. Mandal, O. D. Jayakumar, A. Arya, R. M. Kadam, A. Dixit, R. Naik and A. K. Tyagi, *Inorg. Chem.*, 2011, **50**, 11765–11772.
24 F. N. Sayed, B. P. Mandal, O. D. Jayakumar and A. K. Tyagi, *AIP Adv.*, 2013, **3**, 072133.
25 C. Zhao, S. Feng, R. Xu, C. Shi and J. Ni, *Chem. Commun.*, 1997, 945–946.
26 R. Lebullenger and M. Poulain, *J. Non-Cryst. Solids*, 1995, **184**, 166–171.

27 M. Hidaka, J. F. Scott and J. S. Storey, *Physica B+C*, 1984, **123**, 291–299.
28 Q. Luo, X. Fan, X. Qiao, H. Yang, M. Wang and X. Zhang, *J. Am. Ceram. Soc.*, 2009, **92**, 942–944.
29 N. Kodama, K. Tanaka, T. Utsunomiya, Y. Hoshino, F. Marumo, N. Ishizawa and M. Kato, *Solid State Ionics*, 1984, **14**, 17–24.
30 Y. X. Zhou, Q. Zhang, J. Y. Gong and S. H. Yu, *J. Phys. Chem. C*, 2008, **112**, 13383–13389.
31 R. W. Schwartz, *Chem. Mater.*, 1997, **9**, 2325–2340.
32 F. C. Meldrum and H. Cölfen, *Chem. Rev.*, 2008, **108**, 4332–4432.
33 S. H. Yu, H. Cölfen, A. W. Xu and W. Dong, *Cryst. Growth Des.*, 2004, **4**, 33–37.
34 H. Groen and K. J. Roberts, *J. Phys. Chem. B*, 2001, **105**, 10723–10730.
35 L. Yin, D. Wang, J. Huang, G. Tan and H. Ren, *Mater. Sci. Semicond. Process.*, 2015, **30**, 9–13.
36 C. Jiang and W. Li, *Mater. Lett.*, 2014, **122**, 133–138.
37 Y. Chen, G. Ou, F. Li and T. H. Li, *J. Fluorine Chem.*, 2015, **175**, 121–124.